


[View Journal Online](#)
[View Article Online](#)

Imino-pyridyl and PPh₃ mixed ligand complexes of Cu(I)X (X: I, Br, and Cl): Synthesis, structure, DFT and Hirshfeld surface studies

 Jahangir Mondal , Amit Kumar Manna  and Goutam Kumar Patra *

 Department of Chemistry, Guru Ghasidas Vishwavidyalaya, Bilaspur, Chhattisgarh, 495009, India
 mailtobapi88@gmail.com (J.M.), amitmanna51@gmail.com (A.K.M.), goutam.patra@gu.ac.in (G.K.P.)

 * Corresponding author at: Department of Chemistry, Guru Ghasidas Vishwavidyalaya, Bilaspur, Chhattisgarh, 495009, India.
 e-mail: goutam.patra@gu.ac.in (G.K. Patra).

RESEARCH ARTICLE



doi 10.5155/eurjchem.11.4.334-341.2037

 Received: 30 August 2020
 Received in revised form: 10 October 2020
 Accepted: 20 October 2020
 Published online: 31 December 2020
 Printed: 31 December 2020

KEYWORDS

 DFT
 Imino-pyridyl ligand
 X-ray crystal structure
 Hirshfeld surface studies
 Bridged copper(I) complexes
 Copper(I) coordination polymer

ABSTRACT

Three new halide bridged copper(I) complexes [Cu₂(μ-L)(μ-X)₂](PPh₃)₂ (X: I (1), Br (2) and Cl (3)) have been synthesized by the reaction of Cu(I)X (X: I, Br and Cl) with PPh₃ and the polydentate imino-pyridyl ligand L. Interestingly, copper(I) forms coordination polymers with the ligand L and the co-ligand PPh₃. These complexes 1, 2 and 3 have been characterized by elemental analysis, IR, UV-Vis, and NMR spectroscopy. The crystal structure of the complex 2 has been determined by single-crystal X-ray analysis. Crystal data for complex 2: triclinic, space group *P*-1 (no. 2), *a* = 9.471(10) Å, *b* = 11.043(11) Å, *c* = 13.215(18) Å, α = 65.853(18)°, β = 69.94(2)°, γ = 67.350(14)°, *V* = 1135(2) Å³, *Z* = 2, *T* = 296.15 K, μ(MoKα) = 2.806 mm⁻¹, *D*_{calc} = 1.535 g/cm³, 4059 reflections measured (3.462° ≤ 2θ ≤ 44.818°), 2639 unique (*R*_{int} = 0.0637, *R*_{sigma} = 0.1621) which were used in all calculations. The final *R*₁ was 0.0700 (*I* > 2σ(*I*)) and *wR*₂ was 0.2207 (all data). Hirshfeld surface analysis of the complex 2 showed H···H, N···H and Br···H interactions of 55.9, 14.4 and 4.1%, respectively. MEP of ligand L reflects the whole molecule is reddish yellow in color because of equally distributed electron density over the molecule. For this reason, the ligand is supramolecularly arranged via -{Cu^{1/2}-μ-X₂} rhomboid core in the complex 2. The ligand L is non-emissive at room temperature in dichloromethane, whereas the complexes 1, 2 and 3 are photoluminescent. DFT and Hirshfeld surface studies have also been performed for complex 2.

 Cite this: *Eur. J. Chem.* 2020, 11(4), 334-341

 Journal website: www.eurjchem.com

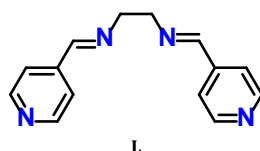
1. Introduction

In recent years, crystal engineering has recognized the intermolecular covalent and non-covalent interactions in terms of self-assembly towards the design of novel functional materials [1-6]. Studies of copper(I) complexes with mixed ligand systems containing triphenyl phosphine and ligands having S and N donors have been increasing because of the flexibility of these ligands and the different steric characteristics of the phosphine ligands, which can modify the compound geometry [7,8]. Copper(I) halides have been used as the inorganic component in the building of novel coordination polymers with diverse structural motifs such as rhomboid fragment, cubane-like or chair-like fragment, one-dimensional ladder strand or zig-zag chain [9]. Cu(I)-complexes are well known for their enriched photoluminescence properties and their potential applications in solar energy conversion, light-emitting devices, luminescence-based sensors, and probes of biological systems [10-15]. Numerous Cu(I)-complexes such as discrete monomers, dimeric clusters and 1D coordination chains have been reported by several researchers [16-18]. Most of the complexes contain halide as the counter anion in combination with triphenylphosphine and N-heterocyclic molecules as the ligand.

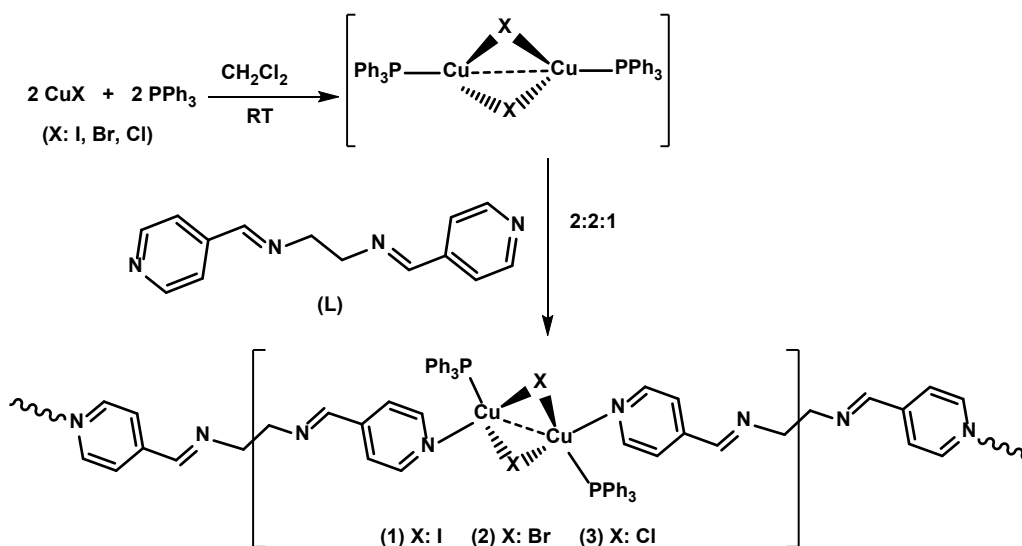
The electronic and structural characteristics of the N-heterocyclic ligands play an important role in determining the structure of the polynuclear complexes and consequently their photophysical properties [19-21]. In addition, the ancillary ligands such as halide and phosphine also have great effects on the emissive properties of the Cu(I)-complexes [22-25].

Analysis of the self-assembly for various intermolecular interactions like hydrogen bonding or π-π stacking is important to understand how molecules interact with their direct environment and focus on insight into crystal packing behavior. Hirshfeld surface-based tools appear as a novel approach to this end [26-31]. The central element in this method is the derivation of the Hirshfeld surface and immediately interpretable visualization of a molecule within its environment, and the decomposition of this surface to provide a directly accessible 2D map [32] as "molecular fingerprint".

In continuation of our studies on the Cu(I) coordination polymers of imino-pyridyl ligands, we have reported here the synthesis, structure, spectroscopic, photophysical, and theoretical studies of halide-based Cu(I) complexes **1**, **2** and **3** of a polydentate imino-pyridyl ligand (L) (Scheme 1).



Scheme 1. Ligand (L) system used in this study.



Scheme 2. Synthetic route of the complexes 1, 2 and 3.

2. Experimental

2.1. Materials and physical measurements

All chemicals used in this study were purchased from Aldrich Chemical Company, USA and Acros Chemical Company, USA, and used without further purification unless otherwise mentioned. The melting point was determined by an electro-thermal IA9000 series digital melting point apparatus and is uncorrected. Microanalyses were carried out using a Perkin-Elmer 2400II elemental analyzer. Infra-red (IR) spectra and solution electronic spectra were recorded on Nicolet Magna IR (Series II) and Shimadzu UV-160A spectrophotometers, respectively. ^1H NMR and ^{13}C NMR and electro-spray ionization mass (ESI-MS) measurements were made using a Bruker Advance 400 MHz and Finnigan LCQ Decap MAX mass spectrometer, respectively. X-ray powder patterns are collected on a Philips PW-1710 automated diffractometer. Fluorescence spectra were recorded on a Perkin Elmer LS55 Luminescence Spectrometer.

2.2. Synthesis of the imino-pyridyl ligand (L)

The imino-pyridyl ligand (L) has been prepared by following a reported procedure [33]. 1 mL (15 mmol) of distilled ethylenediamine and 2.86 (30 mmol) of freshly distilled 4-pyridinecarboxaldehyde were refluxed in 50 mL of anhydrous methanol for 6 h. On evaporating the solvent, a slightly yellow semi-solid was obtained which on recrystallization from *n*-hexane gave colourless needles suitable for X-ray analysis.

(1*E*, 1'*E*)-*N*, *N'*-(ethane-1, 2-diyl) bis(1-(pyridin-4-yl)methanimine) (L): Color: Colorless. Yield: 61%. M.p.: 125-128 °C. FT-IR (KBr, ν , cm^{-1}): 1648 (C=N). ^1H NMR (400 MHz, CDCl_3 , δ , ppm): 8.66 (d, $J = 4$ Hz, 4H, Ar-H), 8.25 (s, 2H, CH), 7.53 (d, $J = 4$ Hz, 4H, Ar-H), 4.03 (s, 4H, CH_2). ^{13}C NMR (200 MHz, CDCl_3 , δ , ppm): 160.84, 150.42, 142.63, 121.83, 61.27. Anal. calcd. for

$\text{C}_{14}\text{H}_{14}\text{N}_4$: C, 70.57; H, 5.92; N, 23.51. Found: C, 70.43; H, 5.92; N, 23.62%. UV/Vis (CH_3OH , λ_{max} , nm, ϵ): 236 (27.30).

2.3. Synthesis of $[\text{Cu}_2(\mu\text{-L})(\mu\text{-I})_2(\text{PPh}_3)_2]_n$ (1)

To a solution of triphenylphosphine (0.262 g, 1 mmol) in CH_2Cl_2 (60 mL), solid cuprous iodide (0.19 g, 1 mmol) was added. The reaction mixture was stirred for 1 h to get a clear colorless solution. The 30 mL CH_2Cl_2 solution of the ligand, L (0.119 g, 0.5 mmol) was added with constant stirring for another 1 h at room temperature to give a clear reddish solution. The solution was evaporated to dryness to obtain a reddish-yellow solid. It was washed with 5 mL of CH_2Cl_2 (Scheme 2).

$[\text{Cu}_2(\mu\text{-}(1E, 1'E)\text{-N, N'-(ethane-1, 2-diyl)bis(1-(pyridin-4-yl)methanimine))(\mu\text{-I})_2(\text{PPh}_3)_2]_n$ (1): Color: Reddish yellow. Yield: 85%. M.p.: >200 °C. FT-IR (KBr, ν , cm^{-1}): 1610 (C=N). Anal. calcd. for $\text{C}_{50}\text{H}_{44}\text{Cu}_2\text{I}_2\text{N}_4\text{P}_2$: C, 52.51; H, 3.88; N, 4.90. Found: C, 52.63; H, 4.13; N, 4.71%. UV/Vis (CH_3OH , λ_{max} , nm, ϵ): 370 (2.33).

2.4. Synthesis of $[\text{Cu}_2(\mu\text{-L})(\mu\text{-Br})_2(\text{PPh}_3)_2]_n$ (2)

To a solution of triphenylphosphine (0.262 g, 1 mmol) in CH_2Cl_2 (60 mL), solid cuprous bromide (0.144 g, 1 mmol) was added. The reaction mixture was stirred for 1 h to get a clear orange solution. The 30 mL CH_2Cl_2 solution of the ligand, L (0.119 g, 0.5 mmol) was added with constant stirring for another 1 h at room temperature to give a clear orange solution. The solution was evaporated to dryness to obtain orange solid. It was washed with 5 mL of CH_2Cl_2 . Bright red single crystals of the complex, suitable for X-ray analysis were obtained by direct diffusion of hexane to the CH_2Cl_2 solution of the yellow solid (Scheme 2).

$[\text{Cu}_2(\mu\text{-}(1E, 1'E)\text{-N, N'-(ethane-1, 2-diyl)bis(1-(pyridin-4-yl)methanimine))(\mu\text{-Br})_2(\text{PPh}_3)_2]_n$ (2): Color: Bright red. Yield: 89%. M.p.: >200 °C. FT-IR (KBr, ν , cm^{-1}): 1607 (C=N). Anal. calcd. for

C₅₀H₄₄Cu₂Br₂N₄P₂: C, 57.21; H, 4.22; N, 5.34. Found: C, 56.98; H, 4.33; N, 5.27%. UV/Vis (CH₃OH, λ_{max}, nm, (ε)): 366 (2.32).

2.5. Synthesis of [Cu₂(μ-L)(μ-Cl)₂(PPh₃)₂]_n (3)

To a solution of triphenylphosphine (0.131 g, 0.5 mmol) in CH₂Cl₂ (30 mL), solid cuprous chloride (0.049 g, 0.5 mmol) was added. The reaction mixture was stirred for 1 h to get a clear reddish solution. The 20 mL CH₂Cl₂ solution of the ligand, **L** (0.60 g, 0.25 mmol) was added with constant stirring for another 1 h at room temperature to give a clear red solution. The solution was evaporated to dryness to obtain a reddish-yellow solid. It was washed with 5 mL of CH₂Cl₂ (Scheme 2).

[Cu₂(μ-(1*E*,1'*E*)-*N,N'*-(ethane-1,2-diyl)bis(1-(pyridin-4-yl)met hanimine))(μ-Cl)₂(PPh₃)₂]_n (**3**): Color: Reddish Yellow. Yield: 80%. M.p.: >200 °C. FT-IR (KBr, ν, cm⁻¹): 1619 (C=N). Anal. calcd. for C₅₀H₄₄Cu₂Cl₂N₄P₂: C, 62.50; H, 4.62; N, 5.83. Found: C, 62.48; H, 4.73; N, 5.74%. UV/Vis (CH₃OH, λ_{max}, nm, (ε)): 360 (2.32).

2.6. X-Ray crystallography

X-ray single-crystal data are collected using MoKα (λ = 0.7107 Å) radiation on a BRUKER APEX II diffractometer equipped with CCD area detector. Data collection, data reduction, structure solution/refinement are carried out using the software package of SMART APEX [34]. The structures are solved by direct methods (SHELXS-97) and standard Fourier techniques, and refined on F² using full-matrix least-squares procedures (SHELXL-97) using the SHELX-97 package [35] incorporated in WinGX [36]. Generally, non-hydrogen atoms are considered anisotropically. Whenever possible, the hydrogen atoms are located on a difference Fourier map and refined. In other cases, the hydrogen atoms are geometrically fixed.

2.7. Theoretical calculations

Gaussian 09 program [37] has been used for the quantum chemical calculations. The possible ground state structures have been optimized with density functional theory (DFT) at B3LYP/6-311G**and B3LYP/LANL2DZ. GaussView 5 program [38] was used for the visualization of the studied systems.

2.8. Hirshfeld surfaces calculations

For obtaining additional insight into the intermolecular interaction of molecular crystals, Hirshfeld surface analysis helps as a powerful set-up. The size and shape of Hirshfeld surface allow the qualitative and quantitative study and imagining of intermolecular close contacts in molecular crystals [39]. The Hirshfeld surface enclosing a molecule is defined by a set of points in 3D space where the contribution to the electron density from the molecule of interest is equal to the contribution from all other molecules. Molecular Hirshfeld surfaces are built based on electron distribution calculated as the sum of spherical atom electron densities [27,40]. Thus, an iso-surface is obtained, and for each point of the iso-surface, two distances can be defined: *d_e*, the distance from the point to the nearest atom outside to the surface, and *d_i*, the distance to the nearest atom inside to the surface. Furthermore, the identification of the regions of particular importance to intermolecular interactions is achieved by mapping normalized contact distance (*d_{norm}*), expressed as: $d_{norm} = (d_i - r_i^{vdw}) / r_i^{vdw} + (d_e - r_e^{vdw}) / r_e^{vdw}$; where *r_i^{vdw}* and *r_e^{vdw}* are the van der Waals radii of the atoms [26]. The value of *d_{norm}* is negative or positive when intermolecular contacts are shorter or longer than *r_{vdw}*, respectively. The graphical plots of the molecular Hirshfeld surfaces mapped with *d_{norm}* employ the red-white-blue color scheme, where red color indicates the shorter intermolecular

contacts, white color shows the contacts around the *r_{vdw}* separation, and blue color is used to point out the longer contact distances. Due to the symmetry between *d_e* and *d_i* in the expression for *d_{norm}*, where two Hirshfeld surfaces touch, both will display a red spot identical in color intensity as well as size and shape [41]. The mixture of *d_e* and *d_i* in the form of a 2D fingerprint plot provides a summary of intermolecular contacts in the crystal and are in complement to the Hirshfeld surfaces [26]. The information about the intermolecular interactions in the immediate environment of each molecule in the asymmetric unit is achieved by such plots. In addition, the close contacts between particular atom types can be highlighted in so-called resolved fingerprint plots [28], which allow the facile assignment of an intermolecular contact to a certain type of interaction and quantitatively summarize the nature and type of intermolecular contacts. Two additional colored properties (shape index and curvedness) based on the local curvature of the surface can also be specified [42]. The Hirshfeld surfaces are mapped with *d_{norm}*, shape-index, curvedness and 2D fingerprint plots (full and resolved) reported in this manuscript were generated using Crystal-Explorer 3.1 [43].

2.9. Molecular electrostatic potential (MEP)

The molecular electrostatic potential at a given point around a molecule can be defined in terms of total charge distribution of the molecule and relates with dipole moments. It supplies a method to understand the electron density which is useful for determining the electrophilic reactivity and nucleophilic reactivity along with hydrogen-bonding interactions [44,45].

3. Results and discussion

3.1. Syntheses of the complexes 1, 2 and 3

Imino-pyridyl ligand **L** is a 1+2 condensate of ethylene diamine and 4-pyridinecarboxaldehyde. The Cu(I) complexes **1**, **2** and **3** have been synthesized in good yields by reacting **L** with Cu(I)X (X: I, Br and Cl) and PPh₃ in 1:2:2 proportion in dichloromethane solvent at room temperature. The syntheses of the complexes **1**, **2** and **3** are summarized in Scheme 2. These complexes are stable in the solid state for about 2-3 weeks in air.

3.2. Structural description of the complex 2

Single crystal XRD analysis unveils that complex **2** is crystallized in a triclinic *P*-1space group and it is a 1-D coordination polymer. The molecular diagram of the complex is shown in Figure 1. The crystallographic details of complex **2** have been summarized in Table 1, bond lengths and angles of complex **2** have been listed in Table 2 and 3, respectively. Compound **2** consists of two independent Cu(I) ions, two bromide anions, and two triphenylphosphine units with one imino-pyridyl ligand **L**. Each Cu(I) cation shows four coordinated distorted tetrahedral geometry. The three phosphorus-bound benzene rings make dihedral angles of 59.5(2), 70.3(2), and 85.5(2)° with each other. The Cu atom displays tetra-coordination, excluding the central Cu...Cu contact of 2.989 Å, and is coordinated by one phosphorus atom (Cu-P = 2.207(5) Å), one nitrogen atom (Cu-N = 2.041(12) Å) and two bromine atoms (Cu-Br = 2.495(3) and 2.514(3) Å) in a distorted tetrahedral geometry. The angles around Cu atom are 104.1(4)° (Br1-Cu2-N1), 102.5(3)° (Br1'-Cu2-N1), 109.53(15)° (P1-Cu2-Br1), 110.78(14)° (P1-Cu2-Br1'), 122.0(4)° (P1-Cu2-N1) and (symmetry code: *i* 1-x, 1-y, -z). In the crystal packing, there is no intramolecular hydrogen bonding. There exists π-π stacking (distance 3.457 Å). Polymer view of [Cu₂(μ-L)(μ-Br)₂(PPh₃)₂]_n (**2**) has been shown in Figure 2.

Table 1. Crystallographic data and refinement parameters for complex 2.

Compound	$[\text{Cu}_2(\mu\text{-L})(\mu\text{-Br})_2(\text{PPh}_3)_2]_n$
Empirical formula	$\text{C}_{25}\text{H}_{22}\text{BrCuN}_2\text{P}$
Formula weight	524.86
Temperature (K)	296.15
Crystal system	Triclinic
Space group	$P\bar{1}$
a (Å)	9.471(10)
b (Å)	11.043(11)
c (Å)	13.215(18)
α (°)	65.853(18)
β (°)	69.94(2)
γ (°)	67.350(14)
Volume (Å ³)	1135(2)
Z	2
ρ_{calc} (g/cm ³)	1.535
μ (mm ⁻¹)	2.806
F(000)	530.0
Crystal size (mm ³)	0.24 × 0.22 × 0.20
Radiation	MoK α ($\lambda = 0.71073$)
2 θ range for data collection (°)	3.462 to 44.818
Index ranges	$-10 \leq h \leq 9, -10 \leq k \leq 11, -14 \leq l \leq 14$
Reflections collected	4059
Independent reflections	2639 [$R_{\text{int}} = 0.0637, R_{\text{sigma}} = 0.1621$]
Data/restraints/parameters	2639/0/259
Goodness-of-fit on F^2	0.945
Final R indexes [$\geq 2\sigma(I)$]	$R_1 = 0.0700, wR_2 = 0.1685$
Final R indexes [all data]	$R_1 = 0.1688, wR_2 = 0.2207$
Largest diff. peak/hole / (e Å ⁻³)	0.98/-0.58
CCDC no.	1027695

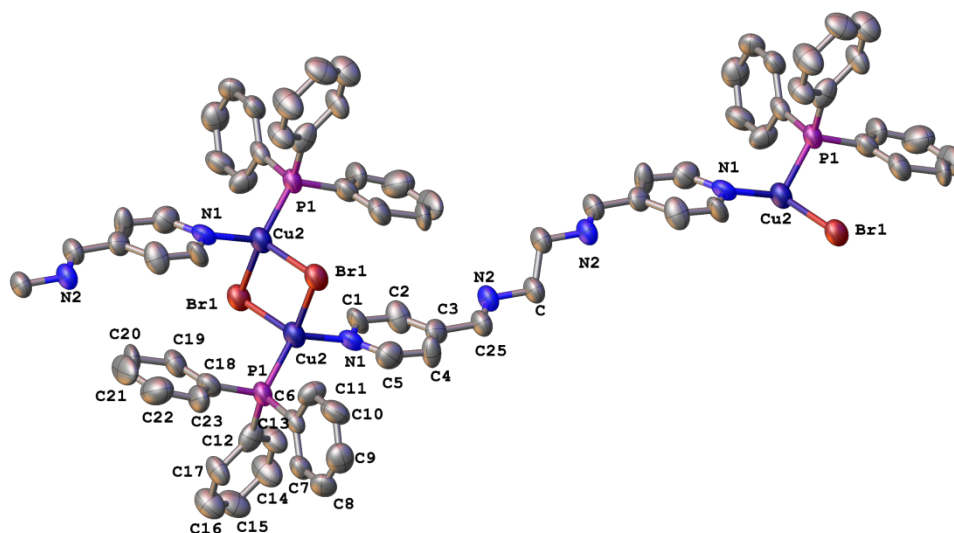
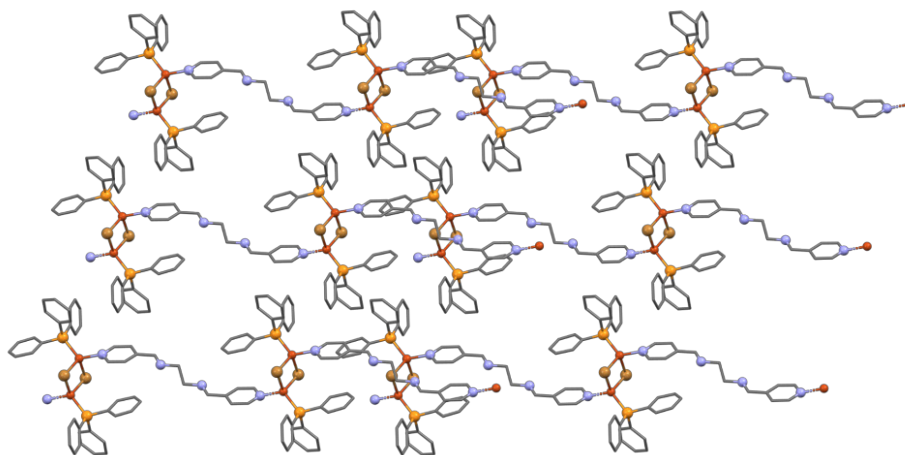
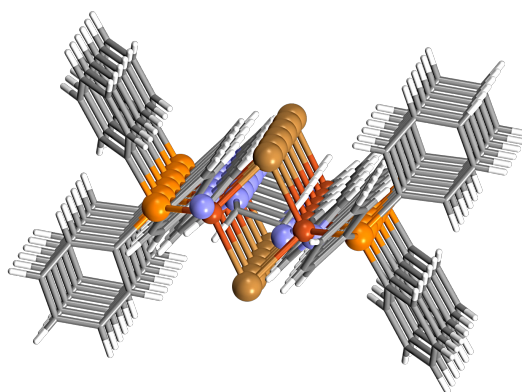
**Figure 1.** Crystal structure of $[\text{Cu}_2(\mu\text{-L})(\mu\text{-Br})_2(\text{PPh}_3)_2]_n$ (2). Thermal ellipsoids are drawn at the 50% probability level.**Figure 2.** Polymeric view of $[\text{Cu}_2(\mu\text{-L})(\mu\text{-Br})_2(\text{PPh}_3)_2]_n$ (2). H atoms are omitted for clarity.

Table 2. Bond distances (Å) for complex 2.

Atom	Atom	Length (Å)	Atom	Atom	Length (Å)
Br1	Cu2	2.495(3)	C8	C9	1.34(2)
Br1	Cu2 ¹	2.514(3)	C9	C10	1.36(2)
Cu2	Br1 ¹	2.514(3)	C10	C11	1.39(2)
Cu2	Cu2 ¹	2.989(5)	C12	C17	1.429(19)
Cu2	P1	2.207(5)	C12	C13	1.347(18)
Cu2	N1	2.041(12)	C17	C16	1.39(2)
P1	C6	1.802(15)	C13	C14	1.358(19)
P1	C12	1.790(16)	C15	C14	1.41(2)
P1	C18	1.814(16)	C15	C16	1.35(2)
N1	C5	1.306(17)	C20	C19	1.41(2)
N1	C1	1.360(17)	C20	C21	1.32(2)
C5	C4	1.381(19)	C18	C23	1.39(2)
C2	C3	1.363(18)	C18	C19	1.41(2)
C2	C1	1.378(19)	C23	C22	1.38(2)
C3	C4	1.347(19)	C21	C22	1.36(2)
C3	C25	1.476(18)	C25	N2	1.257(16)
C6	C7	1.388(18)	N2	C	1.439(16)
C6	C11	1.394(18)	C	C ²	1.48(2)

¹1-x, 1-y, -z; ²3-x, -y, -z.**Table 3.** Bond angles (°) for complex 2.

Atom	Atom	Atom	Angle (°)	Atom	Atom	Atom	Angle (°)
Cu2	Br1	Cu2 ¹	73.25(11)	C7	C6	P1	127.6(12)
Br1	Cu2	Br1 ¹	106.75(11)	C7	C6	C11	116.7(14)
Br1 ¹	Cu2	Cu2 ¹	53.08(7)	C11	C6	P1	115.4(12)
Br1	Cu2	Cu2 ¹	53.67(10)	C9	C8	C7	119.2(15)
P1	Cu2	Br1	109.53(15)	C8	C7	C6	123.2(15)
P1	Cu2	Br1 ¹	110.78(14)	C8	C9	C10	120.6(17)
P1	Cu2	Cu2 ¹	125.28(16)	C9	C10	C11	120.9(16)
N1	Cu2	Br1	104.1(4)	C10	C11	C6	119.2(14)
N1	Cu2	Br1 ¹	102.5(3)	C17	C12	P1	121.7(14)
N1	Cu2	Cu2 ¹	112.7(3)	C13	C12	P1	121.1(14)
N1	Cu2	P1	122.0(4)	C13	C12	C17	117.2(15)
C6	P1	Cu2	116.6(5)	C16	C17	C12	119.8(15)
C6	P1	C18	102.7(7)	C12	C13	C14	124.6(15)
C12	P1	Cu2	111.2(6)	C16	C15	C14	121.4(17)
C12	P1	C6	104.6(7)	C13	C14	C15	117.2(16)
C12	P1	C18	103.4(7)	C15	C16	C17	119.8(16)
C18	P1	Cu2	116.8(5)	C21	C20	C19	119.9(18)
C5	N1	Cu2	125.2(12)	C23	C18	P1	123.8(13)
C5	N1	C1	114.3(14)	C23	C18	C19	119.8(15)
C1	N1	Cu2	118.3(12)	C19	C18	P1	116.4(14)
N1	C5	C4	125.4(16)	C22	C23	C18	119.4(18)
C3	C2	C1	119.5(14)	C18	C19	C20	118.2(16)
C2	C3	C25	119.7(14)	C20	C21	C22	122.6(18)
C4	C3	C2	117.8(15)	C21	C22	C23	120(2)
C4	C3	C25	122.4(16)	N2	C25	C3	122.0(15)
N1	C1	C2	123.4(16)	C25	N2	C	118.2(13)
C3	C4	C5	119.2(16)	N2	C	C2	110.8(15)

¹1-x, 1-y, -z; ²3-x, -y, -z.**Figure 3.** π - π Stacking in complex 2.

The 1-D coordination chains are connected by supra molecular π ... π interactions to form a 3D supramolecular structure (Figure 3).

3.3. Theoretical investigations

B3LYP correlation function by the Gaussian 09 package using a DFT method has been performed to further understand

the electronic structure of the ligand **L**. The optimized structure of ligand **L** has been displayed in Figure 4(a). The energies of some selected molecular orbitals for **L** are shown in Figure 4(b). The energy gaps between HOMO-LUMO, (HOMO-1)-(LUMO+1), (HOMO-2)-(LUMO+2) are 8.2027, 8.3160 and 9.1338 eV for the ligand molecule. The HOMO-LUMO energy gap between the highest occupied molecular orbital and the lowest unoccupied molecular orbital for ligand **L** is 5.30 eV.

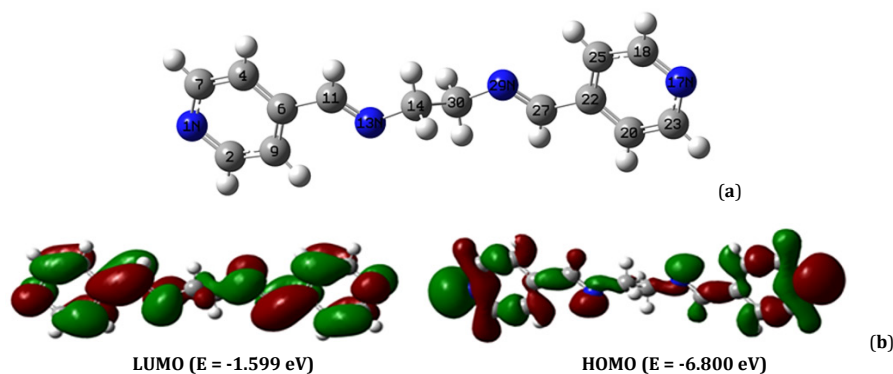


Figure 4. (a) Optimized molecular structure of the ligand L; (b) Surface plots of HOMO and LUMO of the ligand L.

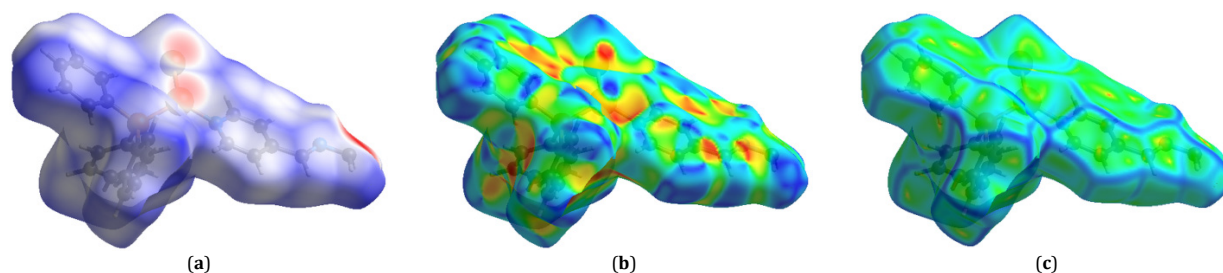


Figure 5. Hirshfeld surfaces of complex 2. (a) 3D d_{norm} surface, (b) surface index, (c) curvedness.

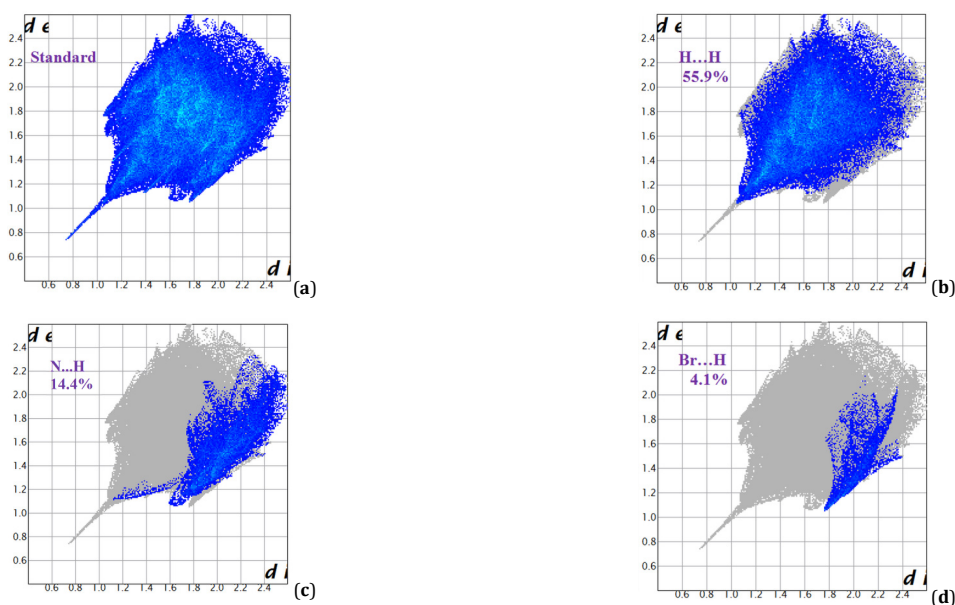


Figure 6. 2D fingerprint plots of complex 2. (a) standard full and (b) resolved into H...H and (c) resolved into N...H (d) Br...H contacts, showing the percentages of contacts contributing to the total Hirshfeld surface area of the molecule.

This value is a useful quantity for examining the kinetic stability. A large energy gap corresponds to a high energy required for electron excitation.

3.4. Molecular Hirshfeld surfaces

The Hirshfeld surface is a suitable tool for describing the surface characteristics of molecules. The molecular Hirshfeld surfaces of complex 2 was generated using a standard (high) surface resolution with the 3D d_{norm} surfaces mapped over a fixed color scale of -0.22 (red) to 1.4 \AA (blue). The shape index mapped in the color range of -0.99 to 1.0 , and curvedness was in the range of -4.0 to 0.4 . The surfaces were shown to be

transparent to allow visualization of the molecular moiety in a similar orientation for all of the structures around which they were calculated. The molecular Hirshfeld surface (d_{norm} , Shape index, and Curvedness) of complex 2 is shown in Figure 5.

The Hirshfeld surface analysis of the complex 2 showed H...H, N...H, and Br...H interactions of 55.9, 14.4, and 4.1% respectively, which revealed that the main intermolecular interactions were H...H intermolecular interactions. The N...H and Br...H interactions were represented by a small area in the left side, whereas the H...H interactions were represented by the largest region in the fingerprint plot (Figure 6) and thus had the most significant contribution to the total Hirshfeld surfaces (55.9%).

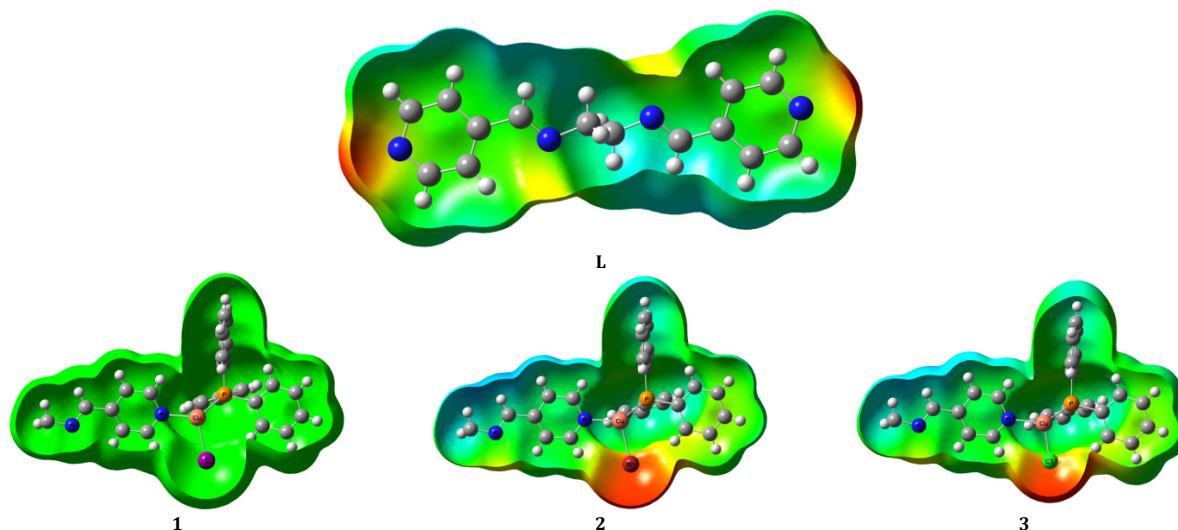


Figure 7. Molecular electrostatic potential (MEP) of ligand (a) L; (b) 1, 2 and 3.

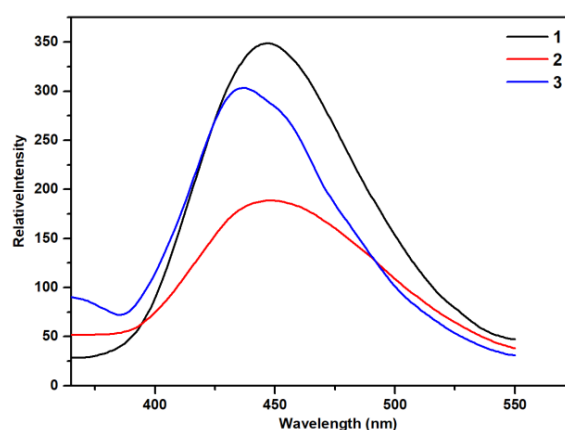


Figure 8. Emission spectra of complexes 1, 2 and 3 in CH_2Cl_2 at room temperature, on excitation at 380 nm.

3.5. Molecular electrostatic potential (MEP)

The potential increases in the order red < yellow < green < blue < pink < white. Red and yellow represents the regions of most negative electrostatic potential which is related to electrophilic reactivity, white represents the regions of most positive electrostatic potential which is related to nucleophilic reactivity and blue represents the region of zero potential. The molecular electrostatic potential (MEP) of ligand **L** is shown in Figure 7(a), the whole molecule is reddish yellow in color because of equally distributed electron density over the molecule. For this reason, the ligand is supramolecularly arranged via $\text{-}\{\text{Cu}^{\text{I}}\text{-}\mu\text{-X}_2\}$ rhomboid core in the complexes **1**, **2**, and **3** (Figure 7(b)).

3.6. Photophysical studies

Fluorescent behaviours of compounds were recorded in 5.0×10^{-5} mol/L CH_2Cl_2 solution at ambient temperature (Figure 8). Complexes **1**, **2**, and **3** have characteristics with the maximum emission at 450, 437, and 447 nm, respectively, upon excitation at 380 nm, whereas the ligand **L** is non-emissive. No emission originating from metal-centered excited states, since they are difficult to oxidize or reduce due to Cu (I) complexes has $3d^{10}$ electron configuration. Therefore, the emission occurred in the complex is attributable to intra-ligand $\pi\text{-}\pi^*$ electronic transitions. The ligand does not show photo-

luminescence because photoinduced intramolecular electron transfer (PET) is prevailing in it. As soon as Cu(I) forms a complex with the ligand and triphenyl phosphine, immediately PET is blocked and the Cu(I) complexes become photoluminescent.

4. Conclusion

Herein, three new halide bridged copper(I) complexes $[\text{Cu}_2(\mu\text{-L})(\mu\text{-X})_2](\text{PPh}_3)_2]_n$ {X: I (**1**), Br (**2**) and Cl (**3**)} have been reported, which were synthesized by reactions of Cu(I)X (X: I, Br and Cl) with PPh_3 and the polydentate imino-pyridyl ligand **L**. The crystal structure of the complex **2** has been determined by single-crystal X-ray analysis and it is 1-D co-ordination polymer. From DFT studies of **L**, it is found that energy gap between the highest occupied molecular orbital and the lowest unoccupied molecular orbital for ligand **L** is 5.30 eV. The Hirshfeld surface analysis of the complex **2** showed H...H, N...H and Br...H interactions of 55.9, 14.4 and 4.1%, respectively. MEP of ligand **L** reflects the whole molecule is reddish yellow in color because of equally distributed electron density over the molecule. For this reason, the ligand is supramolecularly arranged via $\text{-}\{\text{Cu}^{\text{I}}\text{-}\mu\text{-X}_2\}$ rhomboid core in the complex **2**. The ligand **L** is non-emissive at room temperature in dichloromethane, whereas the complexes **1**, **2** and **3** are photoluminescent. The emission in the complexes **1**, **2** and **3** is attributable to intra-ligand $\pi\text{-}\pi^*$ electronic transitions.

Acknowledgements

Goutam Kumar Patra would like to thank the Department of Science and Technology, Government of India, New Delhi for financial support (File Nos. SR/FST/CSI-264/2014 and EMR/2017/0001789).

Supporting information

CCDC-1027695 contains the supplementary crystallographic data for this paper. These data can be obtained free of charge via <https://www.ccdc.cam.ac.uk/structures/>, or by e-mailing data_request@ccdc.cam.ac.uk, or by contacting The Cambridge Crystallographic Data Centre, 12 Union Road, Cambridge CB2 1EZ, UK; fax: +44(0)1223-336033.

Disclosure statement

Conflict of interest: The authors declare that they have no conflict of interest.

Author contributions: All authors contributed equally to this work.

Ethical approval: All ethical guidelines have been adhered.

Sample availability: Samples of the compounds are available from the author.

ORCID


Jahangir Mondal

 <http://orcid.org/0000-0001-9867-5193>

Amit Kumar Manna

 <http://orcid.org/0000-0002-9605-2168>

Goutam Kumar Patra

 <http://orcid.org/0000-0003-3151-0284>

References

- Desiraju, G. R.; In Crystal Engineering: The Design of Organic Solids, Elsevier, Amsterdam, 1989.
- Nangia, A. *J. Chem. Sci.* **2010**, *122*, 295-310.
- Moulton, B.; Zaworotko, M. J. *J. Chem. Rev.* **2001**, *101*, 1629-1658.
- Zaworotko, M. J. *Cryst. Growth Des.* **2007**, *7*, 4-9.
- Aakeroy, C. B.; Beatty, A. M.; Tremayne, M. D.; Rowe, M.; Seaton, C. *Cryst. Growth Des.* **2001**, *1*, 377-382.
- Aakeroy, C. B.; Champness, N. R.; Janiak, C. *Cryst. Eng. Comm.* **2010**, *12*, 22-43.
- Kitaura, R.; Fujimoto, K.; Noro, S.; Kondo, M.; Kitagawa, S. *Angew. Chem.* **2002**, *114*, 141-143.
- Habib, H. A.; Hoffmann, A.; Hoppe, H. A.; Steinfeld, G. *Inorg. Chem.* **2009**, *48*, 2166-2180.
- Caballero, A. B.; Rodriguez-Dieguez, A.; Vieth, J. K.; Salas, J. M.; Janiak, C. *Inorg. Chim. Acta* **2011**, *376*, 674-678.
- Smith, C. S.; Mann, K. R. *Chem. Mater.* **2009**, *21*, 5042-5049.
- Sun, L. N.; Yu, J. B.; Peng, H. S.; Zhang, J. Z.; Shi, L. Y.; Wolfbeis, O. S. *J. Phys. Chem. C* **2010**, *114*, 12642-12648.
- Wang, Y. M.; Teng, F.; Hou, Y. B.; Xu, Z.; Wang, Y. S.; Fu, W. F. *Appl. Phys. Lett.* **2005**, *87*, 233512-233515.
- Tsuboyama, A.; Kuge, K.; Furugori, M.; Okada, S.; Hoshino, M.; Ueno, K. *Inorg. Chem.* **2007**, *46*, 1992-2001.
- Wei, Z. W.; Sun, L. N.; Liu, J. L.; Zhang, J. Z.; Yang, H. R.; Yang, Y.; Shi, L. Y. *Biomaterials* **2014**, *35*, 387-392.
- Liu, Z.; Sun, L. N.; Li, F. Y.; Liu, Q.; Shi, L. Y.; Zhang, D. S.; Yuan, S.; Liu, T.; Qiu, Y. N. *J. Mater. Chem.* **2011**, *21*, 17615-17618.
- Armaroli, N.; Accorsi, G.; Holler, M.; Moudam, O.; Nierengarten, J. F.; Zhou, Z.; Wegh, R.; Welter, R. T. *Adv. Mater.* **2006**, *18*, 1313-1316.
- Zhang, Q.; Zhou, Q.; Cheng, Y.; Wang, L.; Ma, D.; Jing, X.; Wang, F. *Adv. Mater.* **2004**, *16*, 432-436.
- Nishikawa, M.; Nomoto, K.; Kume, S.; Inoue, K.; Sakai, M.; Fuji, M.; Nishihara, H. J. *J. Am. Chem. Soc.* **2010**, *132*, 9579-9581.
- McCormick, T.; Jia, W. L.; Wang, S. *Inorg. Chem.* **2006**, *45*, 147-155.
- Cuttell, D. G.; Kuang, S. M.; Fanwick, P. E.; McMillin, D. R.; Walton, R. A.; *J. Am. Chem. Soc.* **2002**, *124*, 6-7.
- Smith, C. S.; Branham, C. W.; Marquardt, B. J.; Mann, K. R. *J. Am. Chem. Soc.* **2010**, *132*, 14079-14085.
- Mondal, J.; Mukherjee, A.; Patra, G. K.; *Inorg. Chim. Acta* **2017**, *463*, 44-53.
- Mondal, J.; Pal, P. K.; Mukherjee, A.; Patra, G. K. *Inorg. Chim. Acta* **2017**, *466*, 274-284.
- Ghorai, A.; Mondal, J.; Patra, G. K. *J. Mol. Struct.* **2015**, *1097*, 52-60.
- Mondal, J.; Ghorai, A.; Singh, S. K.; Saha, R.; Patra, G. K. *J. Mol. Struct.* **2016**, *1108*, 315-324.
- Hyde, S.; Andersson, S.; Larsson, K.; Blum, Z.; Landh, T.; Lidin, S.; Ninham, B. W. *The Language of Shape*, Elsevier, Amsterdam, 1997.
- Spackman, M. A.; McKinnon, J. J. *CrystEngComm* **2002**, *4*, 378-392.
- McKinnon, J. J.; Fabbiani, F. P. A.; Spackman, M. A. *Cryst. Growth Des.* **2007**, *7*, 755-769.
- Moggach, S. A.; Parsons S.; Wood, P. A. *Crystallogr. Rev.* **2008**, *14*, 143-184.
- Parkin, A.; Barr, G.; Dong, W.; Gilmore, C. J.; Jayatilaka, D.; McKinnon, J. J.; Spackman, M. A.; Wilson, C. C. *CrystEngComm* **2007**, *9*, 648-652.
- Barr, G.; Dong, W.; Gilmore, C. J.; Parkin, A.; Wilson, C. C. *J. Appl. Crystallogr.* **2005**, *38*, 833-841.
- Clark, T. E.; Makha, M.; Sobolev, A. N.; Raston, C. L. *Cryst. Growth Des.* **2008**, *8*, 890-896.
- Mukherjee, A.; Dutta, A.; Jana, A. D.; Patra, G. K. *Inorg. Chim. Acta* **2013**, *404*, 131-143.
- Bruker, SMART, SAINT. Bruker AXS Inc., Madison, Wisconsin, USA, 2012.
- G. M. Sheldrick, *Acta Cryst. A* **2008**, *64*, 112-122.
- Farrugia, L. J. *J. Appl. Crystallogr.* **1999**, *32*, 837-838.
- Frisch, M. J.; Trucks, G. W.; Schlegel, H. B.; Scuseria, G. E.; Robb, M. A.; Cheeseman, J. R.; Montgomery Jr., J. A.; Vreven, T.; Kudin, K. N.; Burant, J. C.; Millam, J. M.; Iyengar, S. S.; Tomasi, J.; Barone, V.; Mennucci, B.; Cossi, M.; Scalmani, G.; Rega, N.; Petersson, G. A.; Nakatsuji, H.; Hada, M.; Ehara, M.; Toyota, K.; Fukuda, R.; Hasegawa, J.; Ishida, M.; Nakajima, T.; Honda, Y.; Kitao, O.; Nakai, H.; Klene, M.; Li, X.; Knox, J. E.; Hratchian, H. P.; Cross, J. B.; Bakken, V.; Adamo, C.; Jaramillo, J.; Gomperts, R.; Stratmann, R. E.; Yazyev, O.; Austin, A. J.; Cammi, R.; Pomelli, C.; Ochterski, J. W.; Ayala, P. Y.; Morokuma, K.; Voth, G.; Salvador, A. P.; Dannenberg, J. J.; Zakrzewski, V. G.; Dapprich, S.; Daniels, A. D.; Strain, M. C.; Farkas, O.; Malick, D. K.; Rabuck, A. D.; Raghavachari, K.; Foresman, J. B.; Ortiz, J. V.; Cui, Q.; Baboul, A. G.; Clifford, S.; Cioslowski, J.; Stefanov, B. B.; Liu, G.; Liashenko, A.; Piskorz, P.; Komaromi, I.; Martin, R. L.; Fox, D. J.; Keith, T.; Al-Laham, M. A.; Peng, C. Y.; Nanayakkara, A.; Challacombe, M.; Gill, P. M. W.; Johnson, B.; Chen, W.; Wong, M. W.; Gonzalez, C.; Pople, J. A.; Gaussian 09W, Gaussian, Inc., Wallingford, CT, 2009.
- Dennington, R.; Keith, T. A.; Millam, J. M. GaussView, Version 5, SemicheM Inc., Shawnee Mission, KS, 2009.
- Norret, M.; Makha, M.; Sobolev, A. N.; Raston, C. L. *New J. Chem.* **2008**, *32*, 808-812.
- Meng, X. Applications of Hirshfeld surfaces to ionic and mineral crystals, PhD. Thesis, University of New England, 2004.
- Pendas, A. M.; Luana, V.; Pueyo, L.; Francisco E.; Sanchez, P. M. *J. Chem. Phys.* **2002**, *117*, 1017-1023.
- Desiraju, G. R. *Angew. Chem. Int. Ed.* **2007**, *46*, 8342-8356.
- Schmidt, G. M. *J. Pure Appl. Chem.* **1971**, *27*, 647-678.
- Sebastin, S.; Sundaraganesan, N. *Spectrochim. Acta A* **2010**, *75*, 941-952.



Copyright © 2020 by Authors. This work is published and licensed by Atlanta Publishing House LLC, Atlanta, GA, USA. The full terms of this license are available at <http://www.eurjchem.com/index.php/eurjchem/pages/view/terms> and incorporate the Creative Commons Attribution-Non Commercial (CC BY NC) (International, v4.0) License (<http://creativecommons.org/licenses/by-nc/4.0>). By accessing the work, you hereby accept the Terms. This is an open access article distributed under the terms and conditions of the CC BY NC License, which permits unrestricted non-commercial use, distribution, and reproduction in any medium, provided the original work is properly cited without any further permission from Atlanta Publishing House LLC (European Journal of Chemistry). No use, distribution or reproduction is permitted which does not comply with these terms. Permissions for commercial use of this work beyond the scope of the License (<http://www.eurjchem.com/index.php/eurjchem/pages/view/terms>) are administered by Atlanta Publishing House LLC (European Journal of Chemistry).